Proceedings World Geothermal Congress 2015
Melbourne, Australia, 19-25 April 2015

Numerical Study of Multi-Fluid and Multi-Level Geothermal System Performance

Martin O. Saar[1, 2], Thomas A. Buscheck[3], Patrick Jenny[4], Nagasree Garapati[2], Jimmy B. Randolph[2], Dimitrios. C. Karvounis[5], Mingjie Chen[3], Yunwei Sun[3], and Jeffrey M. Bielicki[6,7]

[1]Geothermal Energy and Geofluids Group, Department of Earth Sciences, ETH-Zürich, Zürich, CH
[2]Department of Earth Sciences, University of Minnesota, Minneapolis, MN, USA
[3]Atmospheric, Earth, and Energy Division, Lawrence Livermore National Laboratory, Livermore, CA, USA
[4]Institute of Fluid Dynamics, ETH-Zürich, Zürich , CH
[5]Swiss Seismological Service, ETH-Zürich, Zürich, CH
[6]Department of Civil and Geodetic Engineering, The Ohio State University, Columbus, OH, USA
[7]John Glenn School of Public Affairs, The Ohio State University, Columbus, OH, USA
saar@umn.edu

Keywords: Geothermal energy, horizontal wells, parasitic load, working fluid, bulk energy storage, brine, water, CO_2, N_2

ABSTRACT

We introduce the idea of combining multi-fluid and multi-level geothermal systems with two reservoirs at depths of 3 and 5 km. In the *base case,* for comparison, the two reservoirs are operated independently, each as a multi-fluid (brine and carbon dioxide) reservoir that uses a number of horizontal, concentric injection and production well rings. When the shallow and the deep reservoirs are operated in an *integrated* fashion, in the shallow reservoir, power is produced only from the carbon dioxide (CO_2), while the brine is geothermally preheated in the shallow multi-fluid reservoir, produced, and then reinjected at the deeper reservoir's brine injectors. The integrated reservoir scenarios are further subdivided into two cases: In one scenario, both brine (preheated in the shallow reservoir) and CO_2 (from the surface) are injected separately into the deeper reservoir's appropriate injectors and both fluids are produced from their respective deep reservoir producers to generate electricity. In the other scenario, only preheated brine is injected into, and produced from, the deep reservoir for electric power generation. We find that integrated, vertically stacked, multi-fluid geothermal systems can result in improved system efficiency when power plant lifespans exceed ~30 years. In addition, preheating of brine before deep injection reduces brine overpressurization in the deep reservoir, reducing the risk of fluid-induced seismicity. Furthermore, CO2-Plume Geothermal (CPG) power plants in general, and the multi-fluid, multi-level geothermal system described here in particular, assign a value to CO2, which in turn may partially or fully offset the high costs of carbon capture at fossil-energy power plants and of CO2 injection, thereby facilitating economically feasible carbon capture and storage (CCS) operations that render fossil-energy power plants green. From a geothermal power plant perspective, the system results in a CO2 sequestering geothermal power plant with a negative carbon footprint. Finally, energy return on well costs and operational flexibility can be greater for integrated geothermal reservoirs, providing additional options for bulk and thermal energy storage, compared to equivalent, but separately operated reservoirs. System economics can be enhanced by revenues related to efficient delivery of large-scale bulk energy storage and ancillary services products (frequency regulation, load following, and spinning reserve), which are essential for electric grid integration of intermittently available renewable energy sources, such as wind and solar. These capabilities serve to stabilize the electric grid and promote development of all renewable energies, beyond geothermal energy.

1. INTRODUCTION

Previous studies have numerically investigated the performance of geothermal energy production systems that use carbon dioxide (CO_2) as the subsurface heat extraction fluid (Randolph and Saar, 2011a; 2011b; 2011c; Saar et al., 2012), multiple subsurface heat extraction fluids such as CO_2, nitrogen (N_2), and brine (Buscheck et al., 2013b; 2014a), and multi-level reservoirs that are vertically stacked, but separated (Karvounis and Jenny, 2012; Karvounis, 2013; Karvounis and Jenny, 2014). Here, we integrate these approaches and investigate how a combination of brine and CO_2, and N_2 can be used in multi-level reservoirs to improve the overall performance of the geothermal energy production system on three dimensions: 1) energy extraction and conversion efficiency, 2) reservoir lifetime, and 3) economic performance.

In the following, we describe in Section 2.1 using a subsurface working fluid other than brine, namely CO_2, to extract geothermal energy. We then introduce the concept of using multiple subsurface working fluids in Section 2.2. Multi-level geothermal systems are described in Section 2.3. In Section 3 we introduce the idea of combining multi-fluid and multi-level geothermal systems, where one of the working fluids is CO_2. The numerical methods are described in Section 4 and results are presented in Section 5.

2. BACKGROUND

In this section, we provide some background information on the separate systems, CO_2-Plume Geothermal (Section 2.1), multi-fluid geothermal energy systems (Section 2.2), and multi-level geothermal reservoirs (Section 2.3) that are then combined to one integrated system (Section 3).

2.1 CO_2-Plume Geothermal (CPG)

Brown (2000) was the first to propose using CO_2 as a geothermal working fluid, however only in Enhanced or Engineered Geothermal Systems (EGS) which are typically hydro-fractured or hydro-sheared, low-permeability but hot crystalline basement rocks. Using CO_2 has multiple advantages compared to brine, including: 1) it has a low kinematic viscosity, allowing for effective heat advection despite its relatively low heat capacity; and 2) the thermal expansibility of supercritical CO_2 is much larger than that of brine, generating a much stronger thermosiphon effect through the injection well, the reservoir, and the production well. These and other advantages of CO_2 over brine can reduce or eliminate the need for pumps circulating the underground working fluid through the reservoir (Atrens, et al., 2009; 2010; Adams et al., 2014). Furthermore, CO_2 typically exhibits diminished fluid-mineral

reaction characteristics that are restricted to a narrow region that migrates as the CO_2 plume grows (Luhmann et al., 2014; Tutolo et al., 2014).

CO_2 Plume Geothermal (CPG) differs from employing CO_2 in EGS (Brown, 2000; Pruess, 2006) as CPG extracts heat from sedimentary or stratigraphic basins or reservoirs that have naturally high permeability (Randolph and Saar, 2011a; 2011b; 2011c; Saar et al., 2012; Adams et al., 2014; in review 2014; Garapati et al., in prep 2014) and that are much larger than the artificially generated EGS reservoirs. Consequently, these large reservoirs can hold large amounts of CO_2 that can take up the heat that is widely distributed throughout the reservoir resulting in a significant energy source, despite the relatively low temperatures (~100°C) of such fairly shallow (~3 km) reservoirs. Such stratigraphic reservoirs are common throughout the world (IPCC, 2007) as they exist, for example, below approximately half of North America (Runkel et al., 2007; Coleman and Cahan, 2012; NREL 2014). These reservoirs are also the target of CO_2 capture (from fossil-energy systems) and geologic sequestration or storage (called either CCS or GCS) efforts (Global CCS Institute, 2013) in order to reduce global climate change (IPCC, 2005). Thus, coupling CPG with a CO_2 sequestration project, thereby creating a CO_2 capture utilization and sequestration (CCUS) process, can reduce the costs of geologic CO_2 sequestration by using CO_2 as a resource to generate electricity to drive the sequestration pumps (the thermosiphon of CO_2-based systems should drive the geothermal power cycle) and by selling excess electricity to the grid (Randolph and Saar, 2011b). Thus, this approach results in a CO_2-sequestering geothermal power plant with a negative carbon footprint, or, when viewed from the fossil-energy system perspective, the technology renders fossil-fueled power plants green by enabling economic CCUS.

2.2 Multi-Fluid Geothermal Energy Systems

The multi-fluid geothermal energy system approach injects supplemental fluids (in addition to native brine) to create overpressured reservoir conditions and to provide multiple working fluids for pressure augmentation, energy storage, and energy withdrawal (Buscheck et al., 2014; Buscheck, 2014a; 2014b). Building upon CPG (Randolph and Saar, 2011a; 2011b, 2011c; Saar et al., 2012; Adams et al., 2014; in review 2014; Garapati et al., in prep 2014) described above, the multi-fluid approach injects into subsurface geothermal reservoirs a combination of CO_2 that is captured from the exhaust streams of fossil-energy systems and N_2 that is separated from air (Figures 1 and 2). Fluid-recirculation efficiency and per-well fluid production rates are increased by the additional supplemental fluid and the advantageous thermophysical properties of those fluids, notably, their high mobilities (i.e., low kinematic viscosities) and high thermal coefficients of thermal expansion. Pressure augmentation is improved by the thermosiphon effect (Adams et al., 2014) that results from injecting cold/dense CO_2 and N_2. These fluids are geothermally heated to reservoir temperature, greatly expand, and thus increase the artesian flow of brine and supplemental fluid at the production wells.

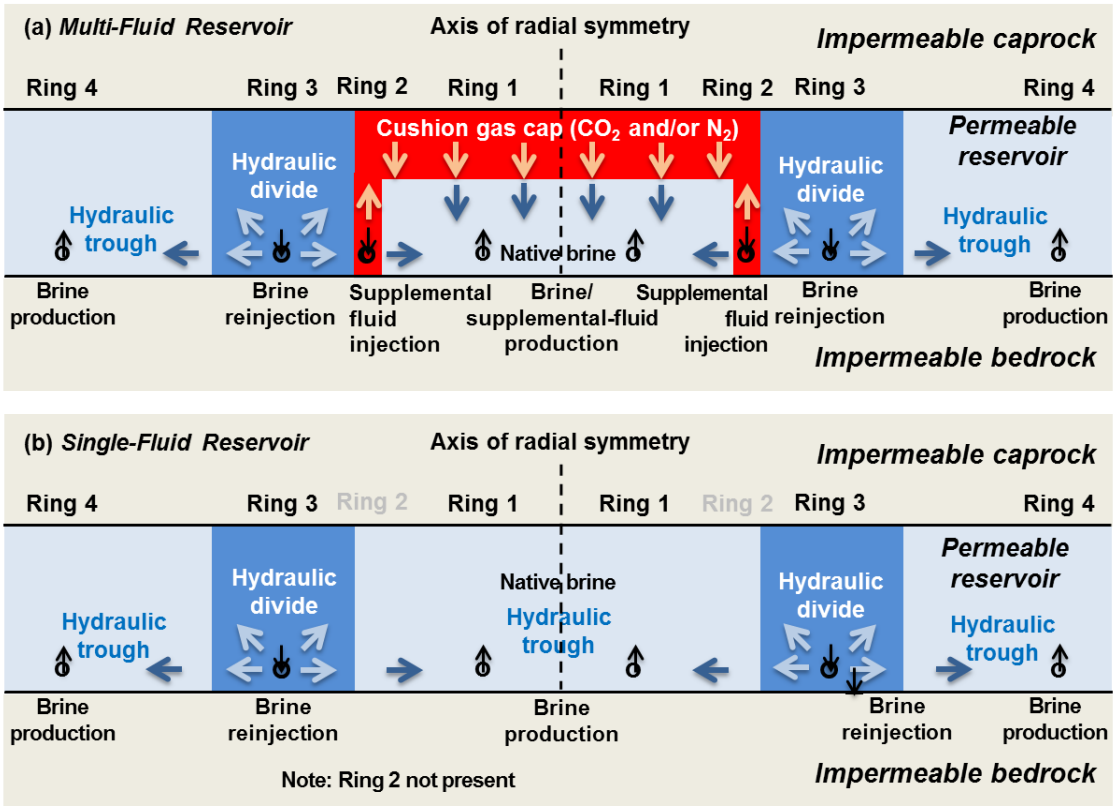

Figure 1: Schematics of multi-ring well-field configurations used in (a) multi-fluid geothermal reservoirs and (b) single-fluid geothermal reservoirs, which are embodiments of geothermal energy systems and methods (Buscheck, 2014a; 2014b). For this study, all wells are located at the bottom of the permeable reservoir formation. Due to buoyancy, supplemental fluid will migrate to the top of the permeable multi-fluid reservoir and form a "cushion gas" cap that increases the pressure-storage capacity of the system. Note that these are not to scale. See Table 1 for well spacings.

Multi-fluid geothermal energy systems use a well pattern consisting of a minimum of four concentric rings of horizontal producers and injectors (Figure 1) that create a hydraulic divide designed to store pressure and supplemental fluids (much like a hydroelectric

dam), segregate the supplemental fluid and brine production zones, and generate large artesian flow rates to better leverage the productivity of horizontal wells. Because fluid production is driven by stored pressure, it is possible to increase production when power demand is high or when there is a deficit of other renewable energy on the grid, such as wind and solar. It may also be advantageous to decrease production when demand is low or when there is a surplus of renewable energy on the grid, which will serve to further store pressure and thermal energy for use when demand is high. The hydraulic divide segregates the inner sweep zone, where brine and supplemental fluid recirculate, from the outer sweep zone, where only brine recirculates.

A key advantageous feature of multi-fluid geothermal energy systems is the option of time-shifting the parasitic load associated with fluid recirculation to achieve bulk energy storage and to provide ancillary services. This parasitic load is dominated by the power required to pressurize and inject brine. By comparison, the power required to compress and inject CO_2 is negligible, while the power required for N_2 injection is about 10–25 % that of brine (Buscheck et al., 2015). Because N_2 can be readily separated from the atmosphere and produced, brine can be temporarily stored in surface holding ponds, both N_2 and brine injection can be scheduled to coincide with periods of low power demand or when there is a surplus of renewable energy on the grid. Time-shifting when these parasitic loads are imposed can reduce the cost of powering the fluid-recirculation system and can also provide bulk energy storage on a diurnal basis or even for periods of weeks to months.

2.3 Multi-Level Geothermal Reservoirs

In a typical geothermal system, hot working fluid is produced from a deep (e.g., 5 km, as investigated here) reservoir, some of the thermal energy of the fluid is converted to electric energy at the surface and the cold fluid is injected back into the deep reservoir. An alternative scenario is to first inject the cold working fluid into a shallow (e.g., 3 km, as investigated here) reservoir, which has the potential of increasing the electric power generation for an additional cost that is disproportional to the increased revenues.

The subsurface temperature in relatively shallow (e.g., 3 km) sedimentary or stratigraphic reservoirs above deep (e.g., 5 km) geothermal reservoirs is of less commercial interest for electric power generation. However, since drilling costs increase non-linearly with depth, shallow reservoirs at the site can offer a none-negligible temperature increase of the working fluid at low cost. By circulating the working fluid first in such a shallow, and thus lukewarm, reservoir and then injecting it into the deep reservoir, the cold front in the deep reservoir propagates more slowly and thus high temperatures of the extracted working fluid, which can more efficiently be converted into electric energy, can be maintained over larger periods of time (Karvounis and Jenny, 2012; Karvounis, 2013; Karvounis and Jenny, 2014).

3. COMBINING MULTI-FLUID AND MULTI-LEVEL GEOTHERMAL SYSTEMS

In this paper, we introduce the idea of combining multi-fluid (Section 2.2) and multi-level (Section 2.3) geothermal systems, where one of the subsurface working fluids is CO_2 (Section 2.1). Figure 2 shows three realizations of multi-level reservoirs with a shallow reservoir at 3 km depth and a deep reservoir at 5 km depth. The system on the left in Figure 2 represents the base case, for comparison purposes, in which the two reservoirs are operated independently of each other, denoted (3+5). In contrast, the center system and the system on the right depict realizations where the shallow and the deep reservoir are integrated, denoted (3/5), as in both systems, brine, that is preheated in the shallow reservoir, is injected into the deep reservoir. These two latter cases are subdivided into one (center system) in which, in addition to brine production, CO_2 is also injected into and produced from the deep reservoir and another one (right system), where only brine is produced from the deep reservoir.

Also shown in Figure 2 are the respective surface power plant systems, where power conversion from CO_2 is always assumed to be implemented in a direct system, where the CO_2 is expanded and cooled directly in the turbine, while the brine system is always an indirect or binary power conversion technology, where the heat from the subsurface working fluid is transferred to a secondary working fluid in a heat exchanger. This choice of system implementation is based on power output optimization considerations as discussed in Adams et al. (2014; in review 2014).

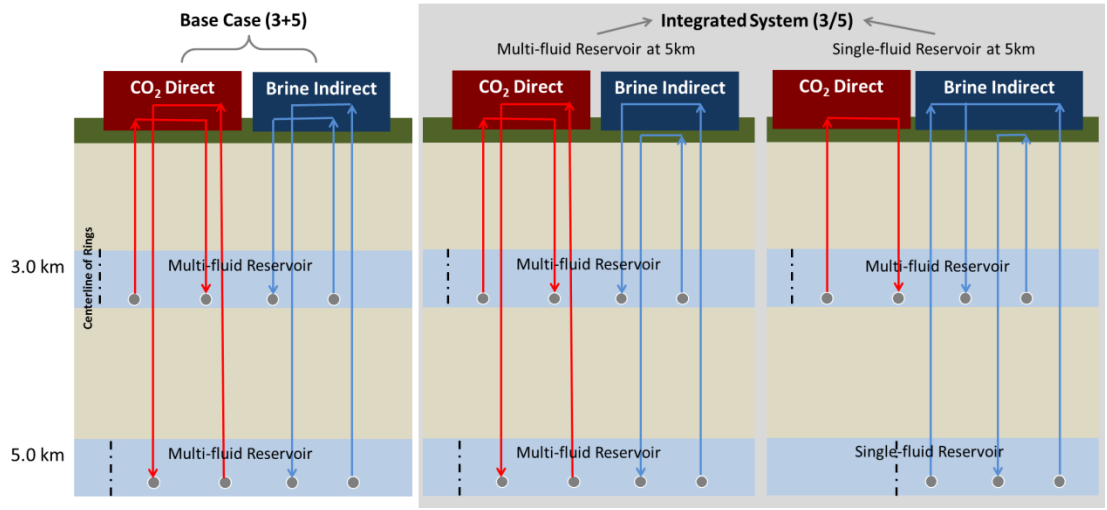

Figure 2: Schematic of the base case and integrated cases for multi-level, multi-fluid or single-fluid reservoirs being investigated. Figure 1 shows the arrangement of the wells and the resultant hydraulic conditions within a reservoir. This figure shows the different arrangements for how the individual reservoirs are connected to each other and the appropriate power plants. The reservoir thickness is 125 m in all cases. "(3+5)" means two independent reservoirs, while "(3/5)" means two integrated reservoirs.

Figure 1 shows the arrangement of the wells and the resultant hydraulic conditions within the reservoirs. Both injection and production wells in both the shallow and the deep reservoirs are concentric, horizontal, arc-shaped wells that are located near the bottom of the reservoir. In the shallow reservoir (Figure 1a), the innermost ring (Ring 1) is a native brine and/or supplmental fluid (here CO_2) production well. Ring 2 is a supplemental fluid injection well. Ring 3 is also an injection well, however, the third ring reinjects brine that is produced from Rings 1 and 4. Well ring radii and footprint areas of the respective thermal sweep areas are given in Table 1. Figure 1b shows the deep reservoir with only brine injection and production which corresponds with the case depicted on the right of Figure 2.

Figure 1 illustrates that in both the shallow and the deep reservoirs, the outermost two rings create a hydraulic brine trough (Ring 4) and a hydraulic brine divide (Ring 3) with the latter being immediately adjacent to the supplemental fluid (in the shallow reservoir) and the brine production (in the deep reservoir). In the shallow and deep multi-fluid reservoirs, this hydraulic brine divide serves to contain and pressurize the supplemental fluid (here CO_2) on the inner side while pressurizing the brine on the outer side, facilitating production of both fluids. In the deep single-fluid reservoir (Figure 1b), the hydraulic brine divide simply pressurizes the brine on both adjacent sides.

Table 1: Four-ring well-field cases considered in this study.

Well-field footprint area (km^2)	Well-ring radius (km)				Inner sweep area (km^2)	Outer sweep area (km^2)
	Ring 1 brine/CO_2 producers	Ring 2 CO_2 injectors	Ring 3 brine injectors	Ring 4 brine producers		
64	0.5	2.0	2.5	4.5	11.8	44.0
64*	0.5	N/A	2.5	4.5	18.9	44.0

Note: *Single-fluid (brine-only) reservoir case (Figure 1b); because this case does not involve CO_2 injection, the CO_2 injectors in Ring 2 are not required. The reservoir thickness is 125 m for all cases.

4. MODELING APPROACH

We conduct reservoir analyses with the Nonisothermal Unsaturated Flow and Transport (NUFT) numerical simulator, which simulates multi-phase heat and mass flow and reactive transport in porous media (Nitao, 1998; Hao et al., 2012). NUFT has been used extensively in reservoir studies of geologic CO_2 sequestration (GCS) and multi-fluid geothermal studies (Buscheck et al., 2012; 2013b; 2013c; 2014; Buscheck, 2014a; 2014b; Buscheck et al., 2015). The values of pore and water compressibility are 4.5×10^{-10} Pa^{-1} and 3.5×10^{-10} Pa^{-1}, respectively. Water density is determined by the ASME (2006) steam tables. The two-phase flow of supercritical CO_2 and water is simulated with the density and compressibility of supercritical CO_2, determined by the correlation of Span and Wagner (1996) and CO_2 dynamic viscosity given by the correlation of Fenghour et al. (1998). The two-phase flow of supercritical N_2 and water is simulated with the density and compressibility for N_2 determined by the correlation of Span et al. (2000) and the dynamic viscosity taken from Lemmon and Jacobsen (2004).

To gain first-order insights, a generic system is modeled over the course of 100 years, consisting of a 125-m-thick reservoir with a permeability of 1×10^{-13} m^2, bounded by low-permeability seal units (caprock and bedrock) each with a permeability of 1×10^{-18} m^2. Hydrologic properties (Table 1 of Buscheck et al., 2015) are similar to previous GCS and multi-fluid geothermal studies (Zhou et al., 2008; Buscheck et al., 2013a; 2013b; 2013c; 2014a; 2014b; Elliot et al., 2013). Because conditions are assumed to be laterally homogeneous, we use a radially symmetric (RZ) model. A geothermal gradient of 37.5°C/km, as well as shallow and deep reservoir bottom depths of 3 and 5 km, respectively, are considered. The initial temperature at the bottom of the reservoir is 127.0°C and 202.0°C for the two depths, respectively, assuming an average surface temperature of 14.5°C. The RZ model is thus a simplified representation of an actual system, but likely representative of rings of arc-shaped horizontal wells, which, in actual geothermal system implementations would likely be horizontal partial-circles or lines that intercept inclined reservoir-caprock interfaces or vertically offset fault interfaces (Garapati et al., in prep. 2014). Using an RZ model allows for fine mesh refinement, particularly around the injectors and producers to better model fluid pressure gradients close to the wells.

For this study, NUFT is used to model pure supercritical CO_2 injection. We use the reservoir model results to determine brine-based, Organic Rankine Cycle (ORC) binary-cycle power generation, using the GETEM code (DOE, 2012). Geothermal energy is extracted from produced CO_2 at the surface using a direct-cycle power system, in which the produced CO_2 is itself sent through a turbine rather than a binary-power system. For CO_2 as a working fluid, direct-power systems offer much greater energy conversion efficiency than binary systems (Adams et al., 2014; in review 2014) because the supercritical fluids generate a substantial pressure difference between the hot production wellhead and the cold injection wellhead, while simultaneously losing considerable temperature during their rise in production wells. The latter effect – Joule-Thomson cooling – causes low binary-system efficiency compared to brine-based systems operating at similar reservoir temperatures (Adams et al., 2014; in review 2014). We assume that produced brine has been separated from the produced CO_2 prior to sending the CO_2 through the turbine to generate electricity. Because the energy penalty for fluid separation is minor, we have neglected it from our power-generation analyses.

Past CPG studies have considered a wide range of CO_2 injection rates (Randolph and Saar, 2011a; Buscheck et al., 2013b; 2013c; 2014a, Adams et al., 2014; in review 2014; Garapati et al., in prep. 2014). For this study, two rates of CO_2 injection into the second concentric ring (Ring 2 in Figure 1a) of horizontal wells are considered: (1) initial rate of 120 kg/sec, gradually increasing to a maximum rate of 240 kg/sec, as produced CO_2 is recirculated to extract more heat from the reservoir and (2) initial rate of 60 kg/sec, increasing (more gradually) to a maximum rate of 120 kg/sec. These scenarios are denoted "120-240" and "60-120" CO_2 injection-rate cases, respectively. All produced CO_2 is reinjected into the second ring of horizontal wells and all produced brine is reinjected into the third ring of horizontal wells (Figures 1a and 2). For the base-case scenarios (with independently operated vertically stacked reservoirs), all produced brine is reinjected into the same reservoir from which it was produced. For the integrated-reservoir scenarios, the brine produced from the 3-km deep reservoir is reinjected into Ring 3 of the 5-km deep reservoir,

and all of the brine produced from the 5-km deep reservoir is reinjected into Ring 3 of the 3-km deep reservoir after it has passed through, and been cooled by, the ORC binary-cycle power plant.

Figure 2 shows a schematic of the different cases being investigated here. The "base case" consists of two *independently* operated 3- and 5-km deep reservoirs. Power is generated from produced CO_2 in a direct system and from brine in an indirect (i.e., binary ORC) system from the shallow reservoir and, separately, from produced CO_2 in a direct system and from brine in an indirect system produced from the deep reservoir. It is assumed that the exit temperature of the brine from the binary-cycle power plant is cooled to 65°C. After CO_2 has passed through the direct-cycle turbine, CO_2 is assumed to have cooled to such a temperature at the injection well head that after compression in the injection well, the temperature of the CO_2 entering the reservoirs at depth is 25°C. The CO_2 that is delivered from the fossil-energy system source is also assumed to enter the reservoirs at 25°C.

For the *integrated* reservoir scenarios, the 3-km deep reservoir is used to preheat brine, prior to that brine being injected into the 5-km deep reservoir; hence, power from the 3-km deep reservoir is only extracted from the produced CO_2 in a direct system. It is assumed that the brine that is preheated and pressurized by the brine injection in the shallow reservoir is driven up the production wells to the ground surface (i.e., under artificially induced artesian conditions) prior to being injected into the 5-km deep reservoir. Directly routing the preheated brine from the shallow reservoir to the deeper reservoir may be preferred, but such a process is not simulated here because of the difficulty in controlling where the injected brine enters the deeper reservoir. The preheated brine injection temperature is initially close to the ambient temperature of the 3-km reservoir, and then declines as heat is extracted from the shallow reservoir. For the 120-240 kg/sec CO_2 injection-rate cases, the temperature of the reinjected brine gradually declines from 127 to 86°C during the course of the 100-yr production period. For the 60-120 kg/sec CO_2 injection rate, less heat is extracted from the 3-km deep reservoir and the temperature of the reinjected brine declines more gradually, from 127 to 91°C over the course of the 100-yr production period. For these integrated reservoir scenarios, the deeper reservoir is operated in two different ways: (1) as a multi-fluid geothermal reservoir (Figure 1a), where both CO_2 and (preheated) brine are injected and produced, and (2) as a single-fluid geothermal reservoir (Figure 1b), where only (preheated) brine is injected and produced.

5. RESULTS AND DISCUSSION

Figure 3 shows the time series of net electric power generation over the course of 100 years of reservoir operations for the six cases considered in this study. Tables 2 and 4 break down the key temperature and pressure metrics, as well as the energy balance (gross, parasitic and net for the respective working fluids) averaged over the first 30 years of production for the 120-240 and 60-120 kg/sec CO_2 injection-rate cases, respectively. Tables 3 and 5 break down that information averaged over 100 years of production. Table 6 compares all six cases considered in this study. Table 7 lists the net power at 100 years for the individual reservoirs that were used to build the composite base-case scenarios and integrated-reservoir scenarios. Table 8 lists the net power at 100 years for the composite cases.

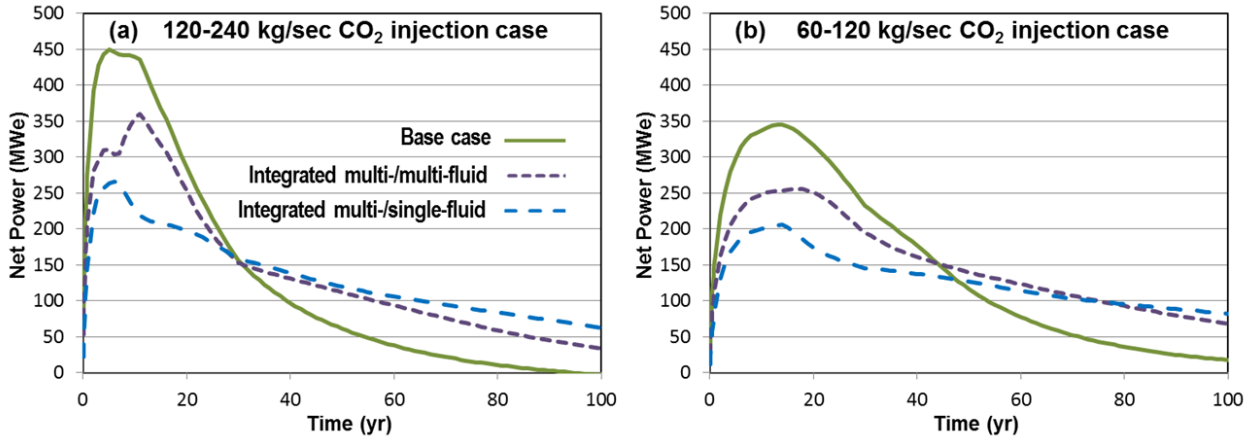

Figure 3: Net electric power time series are plotted for (a) initial and maximum CO_2 injection rates of 120 and 240 kg/sec, respectively, and (b) initial and maximum CO_2 injection rates of 60 and 120 kg/sec, respectively, for cases with shallow (3-km depth) and deep (5-km depth) reservoirs. Time series are plotted for three cases: (1) base case with independently operated shallow and deep multi-fluid reservoirs, (2) integrated multi-/multi-fluid case with integrated shallow and deep multi-fluid reservoirs, and (3) integrated multi-/single-fluid case with a shallow multi-fluid reservoir integrated with a deep single-fluid reservoir. See also Tables 2-5.

The following general observations can be made:

- Higher CO_2 injection rate displaces more brine than lower CO_2 injection rate, resulting in more brine production and reinjection, as well as greater overpressure; all of which produce more gross power (compare Table 3 with Table 5).
- For the base case, power increases strongly with reservoir temperature, with net power for the 5-km deep reservoir being four times greater than that of the 3-km deep reservoir during the first 30 years (Tables 2 and 4) and the first 100 years (Tables 3 and 5).
- Net electric power generation is more efficient for lower CO_2 injection rate (compare Table 4 with Table 2 and Table 5 with Table 3). The primary driver is that the parasitic load of pressurizing brine to reservoir pressure increases strongly

with overpressure, ΔP, in the reservoir. While increased CO_2 injection rate drives more CO_2 and brine to extract more heat from the reservoir and generate more gross power, it also increases the parasitic load.

- Gross brine power is much greater than gross CO_2 power, particularly for the 60-120 kg/sec CO_2 injection rate (Tables 4 and 5); however, net brine power, taking parasitic pumping power requirements into account for the brine cases, can be lower for brine, depending on reservoir depth/temperature and permeability.
- Unit CO_2 value increases with decreasing CO_2 injection rate (Table 6).

Table 2: The power performance for the first 30 years of production is summarized for the cases with initial and maximum CO_2 injection rates of 120 and 240 kg/sec, respectively. The production temperature is at 30 years.

Depth (km)	Brine injection temperature (°C)	Average electric power generation (MWe) over 30 years						Production temperature (°C)		Peak brine injector ΔP (MPa)	Unit CO_2 value ($/tonne)
		Gross brine	Gross CO_2	Gross total	Parasitic total	Net total	Efficiency (%)	Inner ring	Outer ring		
3	65	101.9	3.5	105.4	49.3	56.1	53.2	124.4	114.3	14.34	28.76
5	65	369.2	5.9	375.1	103.9	271.2	72.3	183.7	138.6	15.34	97.04
3 + 5	**65**	**471.1**	**9.4**	**480.5**	**153.2**	**327.3**	**68.1**	**N/A**	**N/A**	**N/A**	**61.49**
3^{c}	65	0.0	3.5	3.5	49.3	-45.8	N/A	124.4	114.3	14.34	N/A
5^{cb}	127-86	367.3	7.1	374.4	62.7	311.7	82.4	193.6	161.2	11.19	108.54
3^{c}/5^{cb}	**127-86**	**367.3**	**10.6**	**377.8**	**111.9**	**265.9**	**70.3**	**N/A**	**N/A**	**N/A**	**55.11**
5^{b}	127-86	275.4	0.0	275.4	24.6	250.8	N/A	195.4	191.8	7.13	N/A
3^{c}/5^{b}	**127-86**	**278.9**	**0.0**	**278.9**	**73.9**	**205.0**	**73.5**	**N/A**	**N/A**	**N/A**	**105.09**

Notes: 3+5 denotes the base case (green) with two independent reservoirs at 3 and 5 km depth, whereas 3/5 indicates two integrated reservoirs at those depths with the lower reservoir being either a multi-fluid (purple) or a single-fluid (only blue) power-producing reservoir. This is also indicated by: 3^{c} denoting an integrated reservoir delivering only CO_2 power from the 3-km deep reservoir; 5^{cb} denoting an integrated reservoir delivering CO_2 and brine power from the 5-km deep reservoir; and 5^{b} denoting an integrated reservoir delivering only brine power from the 5-km deep reservoir. Unit CO_2 value is based on power sales at $100/MWe-hr.

Table 3: The power performance for the first 100 years of production is summarized for the cases with an initial and maximum CO_2 injection rate of 120 and 240 kg/sec, respectively. The production temperature is at 100 years.

Depth (km)	Brine injection temperature (°C)	Average electric power generation (MWe) over 100 years						Production temperature (°C)		Peak brine injector ΔP (MPa)	Unit CO_2 value ($/tonne)
		Gross brine	Gross CO_2	Gross total	Parasitic total	Net total	Efficiency (%)	Inner ring	Outer ring		
3	65	58.3	3.5	61.8	38.4	23.4	37.8	100.4	86.1	14.34	20.77
5	65	160.8	5.4	166.2	63.6	102.6	62.7	119.7	95.3	15.34	51.59
3 + 5	**65**	**219.1**	**9.0**	**228.1**	**102.1**	**126.0**	**55.3**	**N/A**	**N/A**	**N/A**	**40.06**
3^{c}	65	0.0	3.5	3.5	38.4	-34.9	N/A	100.4	86.1	14.34	N/A
5^{cb}	127-86	215.5	7.4	229.9	56.3	173.6	77.9	145.2	118.5	11.19	95.54
3^{c}/5^{cb}	**127-86**	**215.5**	**10.9**	**233.4**	**94.7**	**138.7**	**61.2**	**N/A**	**N/A**	**N/A**	**47.10**
5^{b}	127-86	190.9	0.0	190.9	24.1	166.8	N/A	139.8	141.9	7.13	N/A
3^{c}/5^{b}	**127-86**	**187.4**	**3.5**	**190.9**	**59.0**	**131.9**	**69.1**	**N/A**	**N/A**	**N/A**	**117.08**

Notes: Nomenclature and color coding are the same as for Table 2. Unit CO_2 value is based on power sales at $100/MWe-hr.

Table 4: The power performance for the first 30 years of production is summarized for the cases with an initial and maximum CO_2 injection rate of 60 and 120 kg/sec, respectively. The production temperature is at 30 years.

Depth (km)	Brine injection temperature (°C)	Average electric power generation (MWe) over 30 years						Production temperature (°C)		Peak brine injector ΔP (MPa)	Unit CO_2 value ($/tonne)
		Gross brine	Gross CO_2	Gross total	Parasitic total	Net total	Efficiency (%)	Inner ring	Outer ring		
3	65	80.7	1.1	81.8	27.5	54.3	66.4	125.7	122.2	9.67	34.44
5	65	277.7	0.0	277.7	138.3	239.5	86.2	193.5	177.9	9.68	110.88
3 + 5	**65**	**358.4**	**1.1**	**359.6**	**65.8**	**293.8**	**81.7**	**N/A**	**N/A**	**N/A**	**78.61**
3^{c}	65	0.0	1.1	1.1	27.5	-26.4	N/A	125.7	122.2	9.67	N/A
5^{cb}	127-91	281.2	0.4	281.5	29.6	252.0	89.5	198.1	184.7	7.19	122.18
3^{c}/5^{cb}	**127-91**	**281.2**	**1.5**	**282.6**	**57.1**	**225.6**	**79.8**	**N/A**	**N/A**	**N/A**	**61.97**
5^{b}	127-91	211.8	0.0	211.8	13.8	198.0	93.5	199.5	198.0	3.41	N/A
3^{c}/5^{b}	**127-91**	**211.8**	**1.1**	**13.0**	**41.4**	**171.6**	**80.6**	**N/A**	**N/A**	**N/A**	**108.77**

Notes: Nomenclature and color coding are the same as for Table 2. Unit CO_2 value is based on power sales at $100/MWe-hr.

Table 5: The power performance for the first 100 years of production is summarized for the cases with an initial and maximum CO_2 injection rate of 60 and 120 kg/sec, respectively. The production temperature is at 100 years.

Depth (km)	Brine injection temperature (°C)	Average electric power generation (MWe) over 30 years						Production temperature (°C)		Peak brine injector ΔP (MPa)	Unit CO_2 value ($/tonne)
		Gross brine	Gross CO_2	Gross total	Parasitic total	Net total	Efficiency (%)	Inner ring	Outer ring		
3	65	54.4	1.6	56.0	24.0	32.0	57.2	110.1	91.0	9.67	32.27
5	65	159.8	1.0	160.7	46.1	114.6	71.3	121.1	98.2	11.95	60.38
3 + 5	**65**	**214.2**	**2.6**	**216.8**	**70.1**	**146.7**	**67.7**	**N/A**	**N/A**	**N/A**	**50.72**
3^c	65	0.0	1.7	1.7	24.0	-22.3	N/A	121.1	98.2	9.68	N/A
5^{cb}	127-91	202.8	2.1	204.9	33.3	171.6	83.7	155.3	128.6	7.19	102.07
$3^c/5^{cb}$	**127-91**	**202.8**	**3.8**	**206.6**	**57.3**	**149.3**	**72.3**	**N/A**	**N/A**	**N/A**	**55.79**
5^b	127-91	162.4	0.0	162.4	12.2	150.2	92.5	156.5	158.0	4.42	N/A
$3^c/5^b$	**127-91**	**162.4**	**1.7**	**164.1**	**36.2**	**127.9**	**77.9**	**N/A**	**N/A**	**N/A**	**128.60**

Notes: Nomenclature and color coding are the same as for Table 2. Unit CO_2 value is based on power sales at $100/MWe-hr.

Table 6: Comparison of the power performance of the "3+5" base-case scenarios as well as the "$3^c/5^{cb}$" and "$3^c/5^b$" integrated-reservoir scenarios.

CO_2 injection rate (kg/sec) (initial-max)	Case	Production period (yrs)	Total net energy (GWe-hr)	Average net power (MWe)	Average efficiency (%)	Production temperature (°C) of 5-km deep reservoir		Peak brine injector ΔP (MPa)	Power ratio relative to base case	Unit CO_2 value ($/tonne)
						Inner ring	Outer ring			
120-240	**3 + 5**	**30**	**86,083**	**327.3**	**68.1**	**183.7**	**138.6**	**15.34**	**N/A**	**61.49**
		100	**110,469**	**126.0**	**55.3**	**119.7**	**95.3**	**15.34**	**N/A**	**40.06**
	$3^c/5^{cb}$	**30**	**69,847**	**265.9**	**70.3**	**193.6**	**161.2**	**11.19**	**0.81**	**55.11**
		100	**121,520**	**138.7**	**61.2**	**145.2**	**118.5**	**11.19**	**1.10**	**47.10**
	$3^c/5^b$	**30**	**53,908**	**205.0**	**73.5**	**195.4**	**191.8**	**7.13**	**0.63**	**105.09**
		100	**115,584**	**131.9**	**69.1**	**139.8**	**141.9**	**7.13**	**1.05**	**117.08**
60-120	**3 + 5**	**30**	**77,261**	**293.8**	**81.7**	**193.5**	**177.9**	**9.68**	**N/A**	**78.61**
		100	**128,608**	**146.8**	**67.7**	**121.1**	**98.2**	**11.95**	**N/A**	**50.72**
	$3^c/5^{cb}$	**30**	**59,318**	**225.6**	**79.8**	**198.1**	**184.7**	**9.68**	**0.77**	**61.97**
		100	**130,833**	**149.3**	**72.3**	**155.3**	**128.6**	**7.19**	**1.02**	**55.79**
	$3^c/5^b$	**30**	**45,124**	**171.6**	**80.6**	**199.5**	**198.0**	**3.41**	**0.58**	**108.77**
		100	**112,058**	**127.9**	**77.9**	**156.5**	**158.0**	**4.42**	**0.87**	**128.60**

Notes: Nomenclature and color coding are the same as for Table 2. Unit CO_2 value is based on power sales at $100/MWe-hr.

Table 7: Net power generation at 100 years is listed for the individual reservoirs used to build the composite two-level scenarios.

Reservoir depth	3 km		5 km					
CO_2 injection rate (kg/sec)	**120/240**	**60/120**	**120/240**	**60/120**	**120/240**	**60/120**	**120/240**	**60/120**
Brine injection temperature	**65°C**	**65°C**	**65°C**	**65°C**	**127-86°C**	**127-91°C**	**127-86°C**	**127-91°C**
Multi-fluid or single-fluid	**multi**	**multi**	**Multi**	**multi**	**multi**	**multi**	**single**	**single**
Net power at 100 yr (MWe)	**-4.5**	**9.0**	**1.0**	**8.4**	**65.3**	**89.4**	**94.9**	**103.9**

Notes: The value of CO_2 injection rate for the single-fluid reservoirs pertains to the shallow (3-km depth) multi-fluid reservoir that supplied the preheated brine to that reservoir.

Table 8: Net power generation at 100 years is listed for the composite cases.

	Base-case scenario		Integrated-reservoir scenario			
CO_2 injection rate (kg/sec)	**120/240**	**60/120**	**120/240**	**60/120**	**120/240**	**60/120**
Brine injection temperature	**65°C**	**65°C**	**127-86°C**	**127-91°C**	**127-86°C**	**127-91°C**
Multi-fluid or single-fluid	**Multi/multi**	**Multi/multi**	**Multi/multi**	**Multi/multi**	**Multi/single**	**Multi/single**
Net power at 100 yr (MWe)	**-3.5**	**17.4**	**33.0**	**67.6**	**62.6**	**82.1**

The following comparisons can be made between the integrated-reservoir scenarios and independent reservoir base-case scenarios:

- Net electric power generation after 100 years is much greater for the integrated-reservoir scenarios than it is for the base-case scenarios (Table 8 and Figure 3). Net power at 100 years is particularly high (82.1 MWe) for the integrated multi-fluid/single-fluid reservoir system with a 60-120 kg/sec CO_2 injection rate in the shallow reservoir.
- Net electric power increases more quickly for the base-case scenarios than the integrated-reservoir scenarios, and remains greater than that of the integrated-reservoir scenarios for the first 30 years for a 120-240 kg/sec CO_2 injection rate (Figure 3a).
- Net power increases more quickly for the base-case scenarios than the integrated-reservoir scenarios, and remains greater than that of the integrated-reservoir scenarios for the first 40 years for a 60-120 kg/sec CO_2 injection rate (Figure 3b). For a 60-120 kg/sec CO_2 injection rate, the base case is inherently efficient, with a very slow rate of thermal decline; therefore, it is difficult to improve upon its long-term performance by preheating brine in an integrated-reservoir system.
- The integrated-reservoir scenarios generate less gross power than the base-case scenarios during the first 30 years of production (Tables 2 and 4). It is more effective to directly use produced brine to generate more gross power during early time because the benefit of injecting preheated brine is delayed until reinjected brine has broken through to the production wells.
- The integrated-reservoir scenarios have a higher efficiency because preheated brine has a lower viscosity than the cooled brine (Table 6). Lower viscosity decreases fluid overpressure, ΔP, at the brine injectors, which reduces the parasitic load of pressurizing brine to reservoir conditions.
- For later times (>30 years), the integrated-reservoir scenarios generate more net power because of the greater efficiency resulting from both the reduced viscosity of the preheated brine and the fact that preheated brine results in slower thermal decline, thereby maintaining high production enthalpy (Tables 3 and 5). Thus, depending on how long the integrated system is run past 30 years, the time-integrated power generation of the integrated-reservoir system can significantly surpass that of the independent-reservoir base-case system.
- The lower values of fluid overpressure, ΔP, associated with the 5-km deep reservoir of the integrated-reservoir scenarios may reduce the risk of induced seismicity, which tends to increase with proximity to the crystalline basement. The single-fluid reservoir has less than half the ΔP of the corresponding base-case scenarios (Table 6).
- Unit CO_2 value is much greater for the integrated-reservoir scenario with the 5-km deep reservoir operated as a single-fluid geothermal operation (Table 6), which may help justify the high cost of CO_2 capture from fossil-energy systems.
- The production temperatures for the integrated-reservoir scenarios remain relatively high even after 100 years of operation (Tables 3 and 5). The 5-km deep, single-fluid geothermal reservoir has 100-yr production temperatures of 156.5 and 158^{o}C for the inner and outer production rings, respectively.
- The integrated-reservoir scenarios with a single-fluid 5-km deep geothermal reservoir (Figure 1b) require half of the number of CO_2 injectors as in the multi-fluid scenarios (Figure 1a), which will reduce capital cost. Because the eliminated CO_2 injection wells are in the 5-km deep reservoir, this will further reduce capital cost.
- The integrated-reservoir scenarios allow greater operational flexibility and options for time-shifting brine reinjection, which is an effective means of providing bulk energy storage and ancillary services, such as load following (Edmunds et al. 2014; Buscheck et al., 2015).

The dependence of late-time net power on injected brine temperature is particularly apparent in Table 7, which breaks down the net power at 100 years for each of the individual reservoirs that are used to build the composite two-level base-case and integrated-reservoir scenarios. For example, for the 120-240 kg/sec CO_2 injection rate reservoirs with a brine injection temperature of 65^{o}C, net power is -4.5 MWe for the 3-km deep reservoir, indicating that parasitic power exceeds gross power at 100 years. For the corresponding 5-km deep reservoir, net power is only 1.0 MWe at 100 years. Conversely, for the corresponding reservoirs with a brine injection temperature of 127-86^{o}C, net power is 65.3 and 94.9 MWe for the multi-fluid and single-fluid reservoirs, respectively (Table 7). For the 60-120 kg/sec CO_2 injection rate cases with a brine injection temperature of 127-91^{o}C, net power is 89.4 and 103.9 MWe at 100 years for the multi-fluid and single-fluid cases, respectively. Note that these net power values are greater than those of the corresponding integrated-reservoir scenarios (compare Tables 7 and 8).

The reason that the integrated-reservoir scenarios have a lower net power at 100 years than that of the individual 5-km deep reservoirs is due to the very high parasitic load of the shallow 3-km reservoir that is used to preheat the brine for the deeper reservoir. The high parasitic load of the shallow reservoir thus offsets much of the increased net power it additionally generates in the deeper reservoir.

We also conduct a simple cost analysis to investigate the financial returns for the systems investigated. We assume that the only difference in the costs between the systems arises from the costs to drill the vertical portions of the wells. That is, the direct CO_2 surface power plant and the indirect brine surface power plant cost the same across the scenarios and thus can be neglected in the comparison. Similarly, the extra cost incurred from drilling the horizontal portion of the wells is also assumed to be the same across the cases. As a result, the vertical portions of the wells extending to the different depths are the major contributors to the differences in costs across the cases. We use drilling cost estimates from GETEM (DOE, 2012) for brine wells and augment these costs with the estimates from EPA 2010 for CO_2 wells. That is, each well has a vertical section and then a horizontal section that curves in an arc that extends to a semicircle. Two such wells would be necessary for each ring. We calculate the energy produced (MWe-hr) per estimated dollar of vertical well cost, assuming that two vertical wells are drilled for each horizontal well. Table 9 provides the ratio of the energy return on vertical well cost for the integrated system relative to the base case (3+5) system.

Table 9: Ratio (in %) of the energy return on vertical well cost for the integrated (3/5) system relative to the base case (3+5) system.

CO_2 injection rate (initial-maximum)	120-240 kg/sec		60-120 kg/sec	
Production duration	30 years	100 years	30 years	100 years
(3c/5cb):(3+5)	81%	110%	77%	102%
(3c/5b):(3+5)	75%	126%	70%	105%

In the (3c/5cb):(3+5) comparison of Table 9, no difference in the number of wells drilled between the integrated system and the base case system exists. Therefore, the percentages shown are simply the ratio of the power outputs. In the (3/c/5b):(3+5) comparison, though, the integrated system has one less ring of wells in the 5-km deep reservoir, compared to the base case system. This decrease in relative well cost is beneficial, especially for the 100-year timespans, when the ratio of power slightly favors the integrated system (105%) and for the lower 60-120 kg/sec flow rates, where the ratio of power from the integrated system is only 87% of that of the base case system. Including the difference in costs as described above, the energy return on vertical well costs are 126% and 105%, respectively.

6. CONCLUSIONS

In this contribution, we introduced the idea of combining multi-fluid and multi-level geothermal systems, where, in addition to brine, the other working fluid is CO_2. The two reservoirs are at depths of 3 and 5 km. In the *base case*, the two reservoirs are operated independently, each as a multi-fluid (brine and CO_2) reservoir that employs a number of concentric well rings, comprised of horizontal injection and production wells that separately inject or produce brine or CO_2. When the shallow and deep reservoirs are operated in an *integrated* fashion, electric power directly generated from heat extracted from the shallow reservoir is only the result of CO_2 production. Electric power is also indirectly generated by heat extracted from the shallow reservoir because it is used to geothermally preheat brine; which, after it is produced at the surface, is reinjected into the brine injection ring of the deeper reservoir to delay its thermal depletion. Preheated brine extends the lifetime of the deeper reservoir, allowing it to generate more electricity over a 100-year timeframe. The integrated reservoir scenarios are further subdivided into two cases: In one scenario, both brine (preheated in the shallow reservoir) and CO_2 (from the surface) are injected separately into the deeper reservoir's appropriate injectors and both fluids are produced from their respective deep reservoir producers to generate electricity. In the other scenario, only preheated brine is injected into, and produced from, the deep reservoir for electric power generation. CO_2-based power generation is always a direct system where the CO_2 is directly expanded in a turbine to produce electric power, whereas power generation with brine employs an indirect system such as an Organic Rankine Cycle. Two CO_2 injection rate scenarios are employed, one where the initial injection rate of 120 kg/sec gradually increasing to a maximum rate of 240 kg/sec, as produced CO_2 is recirculated to extract more heat from the reservoir and one where the initial CO_2 injection rate of 60 kg/sec increases to a maximum rate of 120 kg/sec.

We find that, long-term, net power output is greater for the integrated-reservoir systems as the reservoir lifespan of the deeper reservoir is extended by preheating brine in the shallow reservoir, increasing overall system efficiency. Net power at 100 years is particularly high (82.1 MWe) for the integrated-reservoir system that utilizes a multi-fluid (brine and CO_2) shallow reservoir and a single-fluid (preheated brine) deep reservoir with a 60-120 kg/sec CO_2 injection rate in the shallow reservoir. Conversely, over the initial 30 to 40 years of power plant operations, net power generation for the separately-operated reservoir systems outperforms that of the corresponding integrated-reservoir systems for respective CO_2 injection rates of 120-240 kg/sec and 60-120 kg/sec. We also find that the lower values of fluid overpressures associated with the 5-km deep reservoir in the integrated-reservoir scenarios should reduce the risk of fluid-induced seismicity, which tends to increase with depth and proximity to the crystalline basement. In particular, the 5-km deep single-fluid geothermal reservoir in the integrated-reservoir system has less than half the fluid overpressure of the corresponding 5-km deep reservoir in the separately-operated (base-case) reservoir system.

Unit CO_2 value is much greater for the integrated-reservoir system with the 5-km deep single-fluid geothermal reservoir than that of the corresponding, separately-operated reservoir system. This may help justify the high cost of CO_2 capture from fossil-energy systems. Furthermore, the integrated-reservoir systems with a 5-km deep single-fluid geothermal reservoir require half of the number of CO_2 injectors used in the multi-fluid geothermal scenarios, reducing capital cost. Because the eliminated CO_2 injectors are in the deep reservoir, this will further reduce capital cost. Hence, the economics of both the geothermal power plant and carbon capture and storage (CCS) operations are significantly improved when employing the here-described carbon capture utilization and storage (CCUS) operation.

In summary, integrated, vertically stacked, multi-fluid geothermal power systems can result in improved system efficiency, particularly over power plant life spans that exceed approximately 30 years. In addition, preheating of brine before deep injection reduces brine overpressurization in the deep reservoir, thereby reducing the risk of fluid-induced seismicity, which increases with depth and proximity to crystalline basements. From an economic point of view, CO_2-Plume Geothermal (CPG) power plants in general, and the multi-fluid, multi-level geothermal system described here in particular, put a value on CO_2, which in turn may partially, or fully offset the high costs of carbon capture at fossil-energy power plants and of CO_2 injection, thereby facilitating economically feasible carbon capture and storage operations that render fossil-energy power plants, such as coal-fired power plants, green. From a geothermal power plant perspective, the system results in a CO_2 sequestering geothermal power plant with a negative carbon footprint. Finally, energy return on well costs and operational flexibility can be greater for integrated geothermal reservoirs, providing additional options for bulk and thermal energy storage, compared to equivalent, but separately operated reservoirs. System economics may be further enhanced by efficiently delivering large-scale bulk energy storage and ancillary services, which are essential for electric grid integration of intermittently available renewable energy sources, such as wind and solar. These capabilities can serve to stabilize the electric grid and promote increased deployment of the major renewable energy sources, including geothermal energy.

ACKNOWLEDGMENTS

This study was funded by the U.S. Department of Energy (DOE) Geothermal Technologies Office (GTO) under grant number DE-FOA-0000336 and a U.S. National Science Foundation (NSF) Sustainable Energy Pathways (SEP) grant, CHE-1230691. This work was performed under the auspices of the USDOE by Lawrence Livermore National Laboratory (LLNL) under DOE contract DE-AC52-07NA27344. We would also like to thank the Initiative for Renewable Energy and the Environment (IREE), a signature program of the Institute on the Environment (IonE) at the University of Minnesota (UMN), for initial seed funding. M.O.S. also thanks the ETH-Zürich (ETHZ) for its endowment support of the Geothermal Energy and Geofluids Group as well as the George and Orpha Gibson Endowment for its support of the Hydrogeology and Geofluids Group in the Department of Earth Sciences at UMN. Any opinions,

findings, conclusions, or recommendations in this material are those of the authors and do not necessarily reflect the views of the DOE, NSF, IREE, IonE, UMN, ETHZ, or LLNL.

DISCLAIMER

Drs. Randolph and Saar have a significant financial interest, and Dr. Saar has a business interest, in Heat Mining Company LLC, a company that may commercially benefit from the results of this research. The University of Minnesota has the right to receive royalty income under the terms of a license agreement with Heat Mining Company LLC. These relationships have been reviewed and managed by the University of Minnesota in accordance with its conflict of interest policies.

REFERENCES

Adams, B., Kuehn, T.H., Bielicki, J.M., Randolph, J.B., and Saar, M.O.: On the importance of the thermosiphon effect in CO_2-Plume Geothermal (CPG) systems, *Energy*, **69**, (2014), 409-418.

Adams, B.M., Kuehn, T.H., Bielicki, J.M., Randolph, J.B., and Saar, M.O.: A Comparison of Electric Power Output of CO_2 Plume Geothermal (CPG) and Brine Geothermal Systems for Varying Reservoir Conditions, submitted to *Applied Energy*, (2014).

ASME: ASME Steam Tables Compact Edition, ASME, Three Park Avenue, New York, NY, USA, (2006).

Atrens, A.D., Gurgenci, H., and V. Rudolph, V.: CO_2 thermosiphon for competitive geothermal power generation. *Energy & Fuels*, **23**, (2009), 553-557.

Atrens, A.D., Gurgenci, H., and V. Rudolph, V.: Electricity generation using a carbon-dioxide thermosiphon. *Geothermics*, **39**, (2010), 161-169.

Brown, D.W.: A hot dry rock geothermal energy concept using supercritical CO_2 instead of water, *Proceedings of the 25th Workshop on Geothermal Reservoir Engineering*, Stanford University, (2000), 233-238.

Buscheck, T.A., Sun, Y., Chen, M., Hao, Y., Wolery, T.J., Bourcier, W.L., Court, B., Celia, M.A., Friedmann, S.J., and Aines, R.D.: Active CO_2 reservoir management for carbon storage: Analysis of operational strategies to relive pressure buildup and improve injectivity, *International Journal of Greenhouse Gas Control*, **6**, (2012), 230-245.

Buscheck, T.A., Elliot, T.R., Celia, M.A., Chen, M., Sun, Y., Hao, Y., Lu, C., Wolery, T.J., and Aines, R.D.: Integrated geothermal-CO_2 reservoir systems: Reducing carbon intensity through sustainable energy production and secure CO_2 storage, *Energy Procedia* **37**, (2013a), 6587-6594.

Buscheck, T.A., Chen, M., Lu, C. Sun, Y., Hao, Y., Celia, M.A., Elliot, T.R., Choi, H., and Bielicki, J.M.: Analysis of operational strategies for utilizing CO_2 for geothermal energy production, *Proceedings of the 38th Workshop on Geothermal Reservoir Engineering*, Stanford University, Palo Alto, CA, (2013b).

Buscheck, T.A., Chen, M., Hao, Y., Bielicki, J.M., Randolph, J.B., Sun, Y., and Choi, H.: Multi-fluid geothermal energy production and storage in stratigraphic reservoirs, *Proceedings for the Geothermal Resources Council 37th Annual Meeting*, Las Vegas, NV, (2013c).

Buscheck, T.A., Bielicki, J.M., Randolph, J.B., Chen, M., Hao, Y., Edmunds, T.A., Adams, B., and Sun, Y.: Multi-fluid geothermal energy systems in stratigraphic reservoirs: Using brine, N_2, and CO_2 for dispatchable renewable power generation and bulk energy storage, *Proceedings of the 39th Workshop on Geothermal Reservoir Engineering*, Stanford University, Palo Alto, CA, (2014).

Buscheck, T.A.: Systems and methods for multi-fluid geothermal energy systems, US Patent Application filed, (2014a).

Buscheck, T.A.: Multi-fluid renewable geo-energy systems and methods, US Patent Application filed, (2014b).

Buscheck, T.A., Bielicki, J.M., Chen, M., Sun, Y. Hao, Y., Edmunds, T.A., Randolph, J.B., and Saar, M.O.: Multi-fluid sedimentary geothermal energy systems for dispatchable renewable electricity, *Proceedings for the World Geothermal Congress 2015*, Melbourne, Australia, in review, (2015).

Coleman, J.L., and Cahan, S.M.: Preliminary catalog of the sedimentary basins of the United States: U.S. Geological Survey Open-File Report, (2012), 2012-1111, Retrieved from http://pubs.usgs.gov/of/2012/1111/

DOE: GETEM–Geothermal electricity technology evaluation model, August 2012 Beta, USDOE Geothermal Technologies Program, (2012).

Edmunds, T.A., Sotorrio, P., Bielicki, J.M., and Buscheck, T.A.: Geothermal power for integration of intermittent generation, *Proceedings for the Geothermal Resources Council 38th Annual Meeting*, Las Vegas NV, (2014).

Elliot, T.R., Buscheck, T.A., and Celia, M.A.: Active CO_2 reservoir management for sustainable geothermal energy extraction and reduced leakage, *Greenhouse Gases: Science and Technology*, **1**, (2013), 1-16.

Fenghour, A., Wakeham, W.A., and Vesovic, V.: The viscosity of carbon dioxide. *J. Phys. Chem. Ref. Data*, **27** (1), (1998), 31–44.

Garapati N., Randolph, J.B., and Saar M.O.: Brine displacement by CO_2, heat energy extraction rates, and lifespan of an axis-symmetric CO_2 Plume Geothermal system with a vertical injection and a horizontal production well, to be submitted to *Geothermics,* (2014).

Hao, Y., Sun, Y., and Nitao, J.J.: Overview of NUFT: A versatile numerical model for simulating flow and reactive transport in porous media, Chapter 9 in *Groundwater Reactive Transport Models*, (2012), 213-240.

IPCC: IPCC special report on carbon dioxide capture and storage. Prepared by working group III of the Intergovernmental Panel on Climate Change (IPCC). (Metz, B., Davidson, O., de Coninck, H.C., Loos, M., and Meyer, L.A., Eds.). Cambridge University Press: New York, (2005).

IPCC: Climate Change 2007: Mitigation. Contribution of working group III to the fourth assessment report of the Intergovernmental Panel on Climate Change (IPCC). (Metz, B., Davidson, O.R., Bosch, P.R., Dave, R., and Meyer, L.A., Eds.) Cambridge University Press: New York, (2007).

Karvounis, D.C., 2013: Simulations of Enhanced Geothermal Systems with an Adaptive Hierarchical Fracture Representation, *Ph.D. Thesis*, ETH-Zürich, Zürich, Switzerland (2013).

Karvounis, D.C. and Jenny, P.: Modeling of flow and transport for EGS cost optimization problems, *Proceedings of the 37th Workshop on Geothermal Reservoir Engineering*, Stanford University, Palo Alto, CA, (2012).

Karvounis, D.C. and Jenny, P.: Numerical Studies of Combined Shallow and Deep Geothermal Systems. *Proceedings of the 39th Workshop on Geothermal Reservoir Engineering*, Stanford University, Palo Alto, CA, (2014).

Lemmon, E.W. and Jacobsen, R.T.: Viscosity and thermal conductivity equations for nitrogren, oxygen, argon, and air, *International Journal of Geophysics*, **25** (1), (2004), 21-69.

Luhmann, A.J., Kong, X.-Z., Tutolo, B.M., Garapati, N., Bagley, B.C., Saar, M.O., and Seyfried W.E. Jr: Experimental dissolution of dolomite by CO_2-charged brine at 100ºC and 150 bar: Evolution of porosity, permeability, and reactive surface area. *Chemical Geology,* **380**, (2014), 145-160

Nitao, J.J.: "Reference manual for the NUFT flow and transport code, version 3.0," Lawrence Livermore National Laboratory, UCRL-MA-130651-REV-1, Livermore, CA (1998).

NREL: Geothermal power generation: Current and planned nameplate capacity (MW) by state, Retrieved from National Renewable Energy Laboratory (NREL), (2014), http://www.nrel.gov/gis/geothermal.html.

Pruess, K.: Enhanced geothermal systems (EGS) using CO_2 as working fluid–a novel approach for generating renewable energy with simultaneous sequestration of carbon, *Geothermics,* **35**, (2006), 351-367.

Randolph, J.B. and Saar, M.O.: Coupling carbon dioxide sequestration with geothermal energy capture in naturally permeable, porous geologic formations: Implications for CO_2 sequestration. *Energy Procedia*, **4**, (2011a), 2206-2213.

Randolph, J.B. and Saar, M.O.: Impact of reservoir permeability on the choice of subsurface geothermal heat exchange fluid: CO_2 versus water and native brine. *Proceedings for the Geothermal Resources Council 35th Annual Meeting*, San Diego, CA, (2011b).

Randolph, J.B., and Saar, M.O.: Combining geothermal energy capture with geologic carbon dioxide sequestration, *Geophysical Research Letters*, **38**, (2011c).

Runkel, A.C., Miller, J.F., McKay, R.M., Palmer, A.R., and Taylor, J.F.: High-resolution sequence stratigraphy of lower Paleozoic sheet sandstones in central North America: The role of special conditions of cratonic interiors in development of stratal architecture. *Geological Society of America Bulletin*, **119**, (2007), 860-881.

Saar, M.O., Randolph, J.B., and Kuehn, T.H.: Carbon Dioxide-based geothermal energy generation systems and methods related thereto. US Patent Number: 20120001429, international patents pending, (2010).

Span, R. and Wagner, W.: A new equation of state for carbon dioxide covering the fluid region from the triple-point temperature to 1100K at pressures up to 800 MPa. *Journal of Physical and Chemical Reference Data*, **25**, (1996), 1509-1596.

Span, R., Lemmon, E.W., Jacobsen, R.T., Wagner, W., and A. Yokozeki, A.: A reference equation of state for the thermodynamic properties of nitrogen for temperatures from 63.151 to 1000 K and pressures to 2200 MPa, *Journal of Physical and Chemical Reference Data*, **29** (6), (2000), 136-1433.

Tutolo, B.M., Luhmann, A.J., Kong, X.-Z., Saar, M.O., and Seyfried, W.E. Jr: Experimental observation of permeability changes in dolomite at CO_2 sequestration conditions, *Environmental Science and Technology*, **48**, (2014), 2445-2452, http://dx.doi.org/10.1021/es4036946

van Genuchten, M.T.: A closed form equation for predicting the hydraulic conductivity of unsaturated soils. *Soil Science Society of America Journal*, **44**, (1980), 892-898.

Zhou, Q., Birkholzer, J.T., Tsang C-F., and Rutqvist, J.A.: A method for quick assessment of CO_2 storage capacity in closed and semi-closed saline formations. *International Journal of Greenhouse Gas Control*, **2**, (2008), 626-639.